

Ordering kinetics in an fcc A_3B binary alloy model: Monte Carlo studies.

M. Kessler,¹ W. Dieterich,¹ and A. Majhofer²

¹*Fachbereich Physik, Universität Konstanz D-78457 Konstanz, Germany and*

²*Institute of Experimental Physics, Warsaw University ul. Hoża 69, PL-00681 Warszawa, Poland*

(Dated: 24 July 2002)

Using an atom–vacancy exchange algorithm, we investigate the kinetics of the order–disorder transition in an fcc A_3B binary alloy model following a temperature quench from the disordered phase. We observe two clearly distinct ordering scenarios depending on whether the final temperature T_f falls above or below the ordering spinodal T_{sp} , which is deduced from simulations at equilibrium. For shallow quenches ($T_f > T_{sp}$) we identify an incubation time τ_{inc} which characterizes the onset of ordering through the formation of overcritical ordered nuclei. The algorithm we use together with experimental information on tracer diffusion in Cu_3Au alloys allows us to estimate the physical time scale connected with τ_{inc} in that material. Deep quenches, $T_f < T_{sp}$, result in spinodal ordering. Coarsening processes at long times proceed substantially slower than predicted by the Lifshitz–Allen–Cahn $t^{1/2}$ law. Structure factors related to the geometry of the two types of domain walls that appear in our model are found to be consistent with Porod’s law in one and two dimensions.

PACS numbers: 05.50.+q, 64.60.-i, 64.60.Cn

I. INTRODUCTION

Several face–centered cubic binary metallic alloys, like Cu_3Au , Cu_3Pd , Mg_3In , Co_3Pt , etc. exhibit long range order with a $L1_2$ –structure below some specific ordering temperature T_0 . In the $L1_2$ –structure four equivalent phases exist, where one of the four simple cubic sublattices building the fcc–lattice are preferentially occupied by the minority atoms. In studying kinetic processes of phase ordering, the following general considerations must be taken into account:

- (i) The transition is of first order. Hence, for small enough supercoolings the disordered phase remains metastable. Relaxation at short times after a temperature quench is governed by the formation of ordered nuclei, which grow into the disordered matrix. On the other hand, the concept of spinodal ordering has been advanced¹ to characterize the phase ordering processes under large supercoolings.
- (ii) The degeneracy of the ordered phase implies a four–component order parameter, $\Psi = (\psi_0, \psi_1, \psi_2, \psi_3)$. Here, ψ_α with $\alpha = 1, 2, 3$, are non–conserved structural order parameter components coupled to a conserved density, ψ_0 , which describes the concentration of the two atomic species.
- (iii) The antiphase domain structure is anisotropic as a result of the existence of two types of antiphase domain walls: low–energy (type–I) and high–energy (type–II) walls.

Under these conditions a rich spectrum of kinetic processes is to be expected. In particular, there remain still open questions concerning scaling and universality in the late–stage growth kinetics. This has motivated several experimental investigations of ordering after a temperature quench, mostly on Cu_3Au , where direct information

has been obtained from time–resolved X–ray diffraction and neutron scattering. On the other hand, only few theoretical or computer simulation studies on such materials have been reported so far.^{2,3,4} Frontera *et al.*³ have recently simulated the growth of $L1_2$ –ordered domains both within an atom–atom exchange and the more realistic atom–vacancy exchange mechanisms, for quench temperatures below the expected spinodal temperature T_{sp} . A similar model with atom–vacancy exchange (ABV–model) was applied by Kessler *et al.*⁴ to surface–induced kinetic ordering processes near $\text{Cu}_3\text{Au}(001)$.

In this paper we investigate the ordering kinetics in the bulk of such alloys at quench temperatures T_f both below and above T_{sp} . In contrast to earlier Monte Carlo studies of nucleation in Ising–type models^{5,6} we again employ the ABV–model with effective chemical interactions between nearest neighbors on the fcc–lattice. This allows us to compare our results directly with experiments on fcc–alloys, where vacancy–driven processes prevail. In particular, we analyze the nucleation regime, where we find a well defined incubation time that sensitively depends on the depth of the quench, $T_0 - T_f$. Moreover, for $T_f < T_{sp}$, with T_{sp} deduced from static correlations, we observe domain patterns typical to spinodal ordering. In the long–time coarsening regime we extract anisotropic scaling functions. Our model is a limiting case where type–I domain walls have exactly zero formation–energy and therefore are extremely stable. Within our accessible time window we find coarsening exponents which are significantly smaller than the conventional exponent $\alpha = 1/2$ for curvature–driven coarsening.^{7,8}

After shortly explaining our model and simulation techniques in section II, we compare in section III ordering processes that occur for shallow ($T_0 > T_f > T_{sp}$) and deep ($T_f < T_{sp}$) quenches. In section IV we define the incubation time τ_{inc} and investigate its dependence on the depth of the quench. Anisotropic scaling functions are discussed in section V, while section VI contains a

short summary of our results.

II. MODEL AND SIMULATION METHOD

We consider a three-dimensional lattice of $L \times L \times L$ fcc-cells with cubic lattice constant a and periodic boundary conditions in all directions. Unless otherwise stated, we use $L = 128$. Each site, i , of the lattice is occupied either by an atom of type A , an atom of type B , or a vacancy, with an obvious condition that the corresponding occupation numbers fulfill $c_i^A + c_i^B + c_i^V = 1$. In accord with the stoichiometry of the A_3B alloys there are exactly three times as many A atoms present as B atoms. The number of vacancies is chosen small enough so that they do not affect static properties of the system.

In our simplified model⁴ only nearest neighbor atom-atom interactions are taken into account. The corresponding Hamiltonian then reads:

$$H = \sum_{\langle i,j \rangle} [V_{AA}c_i^A c_j^A + V_{BB}c_i^B c_j^B + V_{AB}(c_i^A c_j^B + c_i^B c_j^A)], \quad (1)$$

where the sum is restricted to nearest-neighbor pairs. We are interested here in the transition to the ordered $L1_2$ -structure in which minority atoms (B) predominantly occupy one of the simple-cubic sublattices of the original fcc-lattice. It is then natural to assume $V_{BB} > 0$, $V_{AA} < 0$ and $V_{AB} < 0$. The ground state of the $L1_2$ phase is fourfold degenerate and corresponds to all B -atoms segregated to exactly one of the simple cubic sublattices. For a stoichiometric A_3B -alloy the transition occurs at a temperature $T_0 \simeq 1.83|J|/k_B$, with $J = -\frac{1}{4}(V_{AA} + V_{BB} - 2V_{AB})$ as discussed in Ref. 4 (cf. also Refs. 3,9,10). The ordered phase is characterized by one conserved, scalar order parameter, ψ_0 , related to the composition and three non-conserved order parameter components (ψ_1, ψ_2, ψ_3). These are defined by the following equations:

$$\begin{aligned} \psi_0 &= m_1 + m_2 + m_3 + m_4, \\ \psi_1 &= m_1 - m_2 - m_3 + m_4, \\ \psi_2 &= m_1 - m_2 + m_3 - m_4, \\ \psi_3 &= m_1 + m_2 - m_3 - m_4, \end{aligned} \quad (2)$$

where m_α are the differences of the mean A - and B -occupation numbers, $m_\alpha = \langle c_i^A \rangle - \langle c_i^B \rangle$ for $i \in \alpha$. The index $\alpha = 1 \dots 4$ enumerates the four equivalent simple-cubic sublattices of the fcc-structure. For a homogeneous A_3B alloy, $\psi_0 = 2$. In the disordered phase, $\psi_1 = \psi_2 = \psi_3 = 0$, while the four equivalent ordered phases are described as $(\psi_1, \psi_2, \psi_3)/\bar{\psi} = (-1, 1, 1); (1, -1, 1); (1, 1, -1)$ and $(-1, -1, -1)$, with a temperature-dependent $\bar{\psi}$ ($\bar{\psi} = 2$ at $T = 0$). For a non-homogeneous system Eq. (2) gives the corresponding local order parameters for each (cubic) elementary fcc-cell

in terms of weighted averages of the occupation numbers computed of all sites belonging to the cell. (The weights are taken as the inverse of the numbers of neighboring fcc-cells that “share” the site in question, i. e. functions $1/2$ and $1/8$ are taken for the “face” and “corner” sites, respectively).

As can be seen from Eq. (2), each of the non-conserved components of the order parameter describes a modulation of the B -atom concentration along one of the cubic axes. For example, $\psi_1 \neq 0$ means that the system contains alternating B -enhanced and B -depleted atomic layers along the x -axes. As a consequence of such layer-wise arrangement of B -atoms, the (100) peak shows up in an X-ray diffraction experiment in addition to the (200), (020), (002) and (111) peaks characteristic of the underlying fcc-lattice. Similarly, ψ_2 and ψ_3 -type ordering leads to additional (010) and (001) peaks, respectively.¹¹ For a distance \vec{k} from these superstructure peaks the scattering intensity is described by the structure factors,

$$S_\alpha(\vec{k}, t) = \langle |\Psi_\alpha(\vec{k}, t)|^2 \rangle, \quad (3)$$

which in a non-equilibrium state depend on time t . In Eq. (3), $\Psi_\alpha(k_x, k_y, k_z, t)$ denotes the Fourier transform of the order parameter $\psi_\alpha(x, y, z, t)$, and $\alpha = 1, 2, 3$. The widths of these intensity profiles are determined by the sizes of antiphase domains.¹¹ As mentioned in the Introduction, this system displays two types of antiphase boundaries, low-energy type-I boundaries with no change in the arrangement of nearest neighbors, and high-energy type-II boundaries.¹² Since the Hamiltonian, Eq. (1), involves only nearest neighbor interactions, type-I boundaries in fact have zero energy.¹³

We assume here that the time-evolution of our model occurs only through atom-vacancy exchange processes. In an elementary move we first randomly single out one of the vacancies and, second, we choose at random one of its nearest neighbors occupied by an atom. The standard Metropolis algorithm is then used to decide whether the atom-vacancy exchange for the chosen pair takes place or not. In one Monte Carlo step (MCS), the system completes a series of as many such elementary moves as there are lattice sites in the system, i. e. $4L^3$, so that this time unit does not depend on the actual number of vacancies.

In previous simulations⁴ we have chosen the interaction parameters such that they were consistent with the observed Au-segregation at the Cu_3Au (001)-surface. Following Ref. 4, we take $V_{BB} = -V_{AA} = -V_{AB} > 0$ and assume $c^V \simeq 6.1 \cdot 10^{-6}$ as the mean density of vacancies present in the system.¹⁴ For vacancy concentrations of that order we have verified that both static and kinetic properties are independent of the precise value of c^V . To simulate a sudden quench from high temperatures to a final temperature $T_f < T_0$ we start with a random distribution of atoms at time $t = 0$ and let the system evolve in time at T_f . The ensuing equilibration process is analyzed by calculating energies, structure factors, and other ordering characteristics from averages over 10 independent

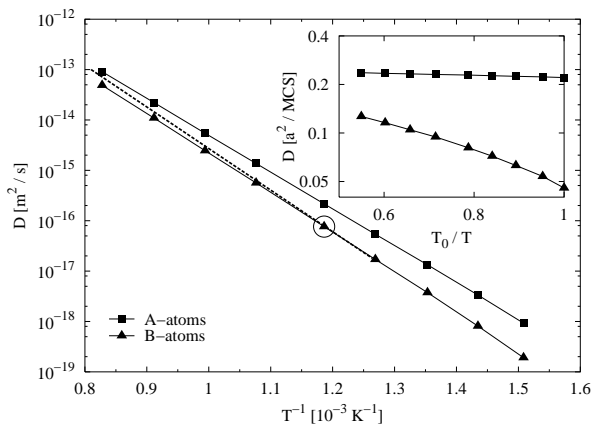


FIG. 1: Tracer diffusion coefficients of A (full squares) and B (full triangles) atoms in an A_3B fcc-alloy. Physical units were assigned to the Monte Carlo data with the help of the experimentally known order-disorder transition temperature, $T_0 = 663$ K, and temperature-dependent concentrations of vacancies¹⁴ in Cu_3Au . The dashed line represents measured Au tracer diffusion coefficients.¹⁶ The open circle marks the experimental point used to set the time scale. In the inset the corresponding “raw” Monte Carlo results are displayed.

Monte Carlo runs.

As the first application of our atom-vacancy exchange algorithm we have calculated tracer diffusion coefficients for A- and B-atoms in the disordered phase close to T_0 . Since in our model $V_{AA} = V_{AB}$, the jump of an A-atom will leave the interaction energy with its environment almost unchanged and hence D_A is found to be nearly temperature-independent. The BB -repulsion, on the other hand, gives rise to a temperature-dependent $D_B < D_A$, see the inset of Fig. 1. As these results refer to a fixed vacancy concentration, they cannot be directly related to experiments, where $c^V(T)$ normally is a strong function of T .¹⁴ Nevertheless, the ratio $D_A/D_B \simeq 2$ at $T/T_0 = 1.7$ very roughly agrees with the experimental value $D_{\text{Cu}}/D_{\text{Au}} \simeq 1.45$ for Cu_3Au at the same T/T_0 -ratio,¹⁵ thus supporting our choice of nearest-neighbor interaction parameters. Moreover, in an attempt to map the Monte Carlo time to the physical time scale, we can exploit experimental knowledge of $c^V(T)$ for Cu_3Au .¹⁴ As $c^V \ll 1$, hopping rates of a tracer atom are simply proportional to c^V . This suggests to introduce a new Monte Carlo time unit $1 \text{ MCS}^* = c^V(T) \cdot 1 \text{ MCS}$, where 1 MCS was defined above as one attempted vacancy exchange per lattice site. Regarding the simulated mean-square displacements as a function of the new time scale (with units MCS^*) allows us to extract diffusion constants D_A and D_B as shown in Fig. 1. Scales on the axes were obtained using the Cu_3Au transition temperature $T_0 = 663\text{K}$, the lattice parameter $a = 3.74\text{\AA}$ and an additional parameter, which is determined by equating the calculated diffusion constant D_B with the experimental D_{Au} at $T/T_0 = 1.27$.¹⁶ The last parameter converts 1 MCS^* directly into seconds. The favorable compari-

son between calculated and measured diffusion constants suggests that the above procedure, based on the atom-vacancy exchange algorithm and the knowledge of the experimental $c^V(T)$ -function, provides a description of processes on the physical time scale. We shall come back to this issue in section III in the context of nucleation processes.

III. THERMALLY ACTIVATED VERSUS CONTINUOUS ORDERING

At $T = T_0$ the model-system defined in the preceding section undergoes a first order phase transition^{3,4,9,10} from the disordered phase (for $T > T_0$) to the $L1_2$ -type ordered structure (for $T < T_0$). The correlation length of the disordered phase, ξ , remains finite at coexistence, and approximately fulfills the mean-field type relation $\xi^2(T) \propto 1/(T - T_{sp})$, with $T_{sp} < T_0$. In our previous work⁴ we found $T_{sp} = (0.967 \pm 0.003)T_0$ as the value best fitting our Monte Carlo data for the correlation length above T_0 . Hence, within this procedure, our model displays a fairly well-defined temperature for the onset of spinodal ordering. A precise separation of the metastable (thermally activated ordering) from the unstable regime (continuous ordering), however, does not exist in systems with short-range interactions.^{5,17}

Below we demonstrate the role of that temperature deduced from equilibrium considerations, in non-equilibrium ordering processes. It turns out that for temperatures $T_f > T_{sp}$ and $T_f < T_{sp}$ two contrasting transition scenarios occur that lead to domain patterns typical of nucleation and spinodal ordering, respectively. We shall illustrate this by one example for each regime.

Let us start our description with thermally activated growth of the ordered phase, i. e. with the case of a shallow quench, $T_0 > T_f > T_{sp}$. We then expect that the ordered regions – nuclei of the new phase – are repeatedly formed and destroyed by thermal fluctuations unless a nucleus exceeding a certain critical size is built. Once formed, such an overcritical nucleus will grow relatively fast against the surrounding disordered bulk until it meets another (growing) ordered domain. An xy -section of a configuration with overcritical nuclei formed in a system of $128 \times 128 \times 128$ fcc-cells is shown in Figs. 2a and 2b. It emerged 7000 MCS after the quench to $T_f = 0.972 T_0 > T_{sp}$. The central nucleus seen in the figure is in fact composed of three “twinned” crystallites, corresponding to $\psi_1 \simeq 2$ (the large, nearly homogeneous, bright spot in Fig. 2a) and $\psi_1 \simeq -2$ (the neighboring dark spot). As shown in Fig. 2b, the homogeneous bright spot of Fig. 2a is in fact composed of two crystallites corresponding to $\psi_3 \simeq -2$ and $\psi_3 \simeq 2$, respectively. A second nucleus characterized by $\psi_1 \simeq 2$ and $\psi_3 \simeq -2$ grows at the right edge of the system. The configuration displayed in Figure 2 is quite typical for a quench temperature slightly above T_{sp} .

To follow the ordering process that takes place in the

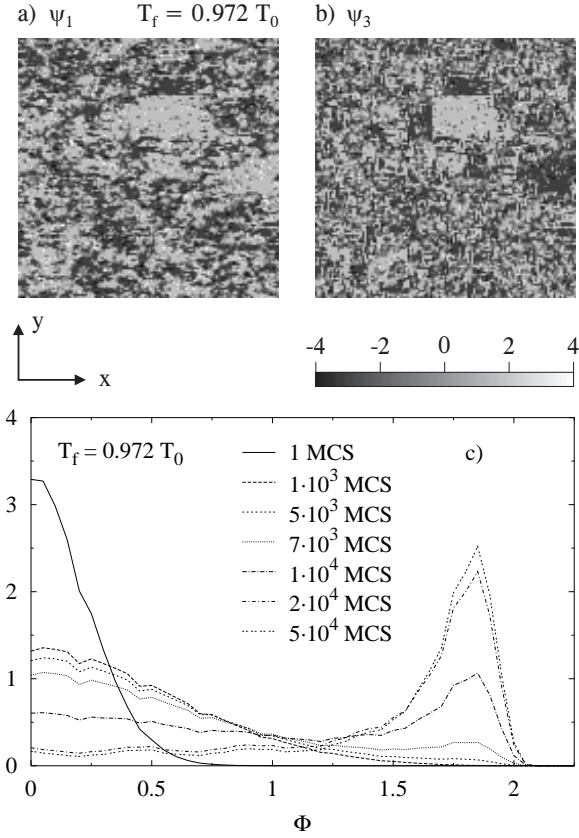


FIG. 2: Thermally activated ordering in a system of $128 \times 128 \times 128$ fcc-cells at $T_f = 0.972 T_0 > T_{sp}$. (a) ψ_1 and (b) ψ_3 patterns containing overcritical nuclei at a time $t = 7 \times 10^3$ MCS after the quench from random initial conditions (grey scales indicate local values of ψ_α ($\alpha = 1, 3$) between -4 and 4). (c) Histograms of corresponding $\Phi = (|\psi_1| + |\psi_2| + |\psi_3|)/3$ values averaged over blocs of $4 \times 4 \times 4$ fcc-cells calculated at a series of times after the quench.

whole volume of the system we now introduce an additional quantity³ $\Phi = (|\psi_1| + |\psi_2| + |\psi_3|)/3$ as a convenient indicator of the degree of local order: $\Phi \simeq 0$ in the disordered phase and $\Phi \leq 2$ for any of the four equivalent ordered states. Further, we divide the system into blocs of $4 \times 4 \times 4$ fcc-cells, calculate Φ independently for each bloc to obtain a distribution function $P(\Phi, t)$ for a series of time intervals after the quench. For a quench to $T_f = 0.972 T_0$ the obtained histograms are shown in Fig. 2c. In this figure we easily identify three stages of the ordering process. First, up to several thousand MCS, the whole system remains disordered. The distribution of Φ broadens with time but stays concentrated close to $\Phi = 0$. Then, after some incubation time, τ_{inc} , see section IV, the second maximum close to $\Phi = 2$ shows up. At that moment first overcritical nuclei emerge in the system and start to grow. The second stage, in which overcritical nuclei grow against the disordered bulk, is realized by histograms for $7 \cdot 10^3 \leq t \leq 10^4$ MCS in which both peaks are clearly visible. In the third stage,

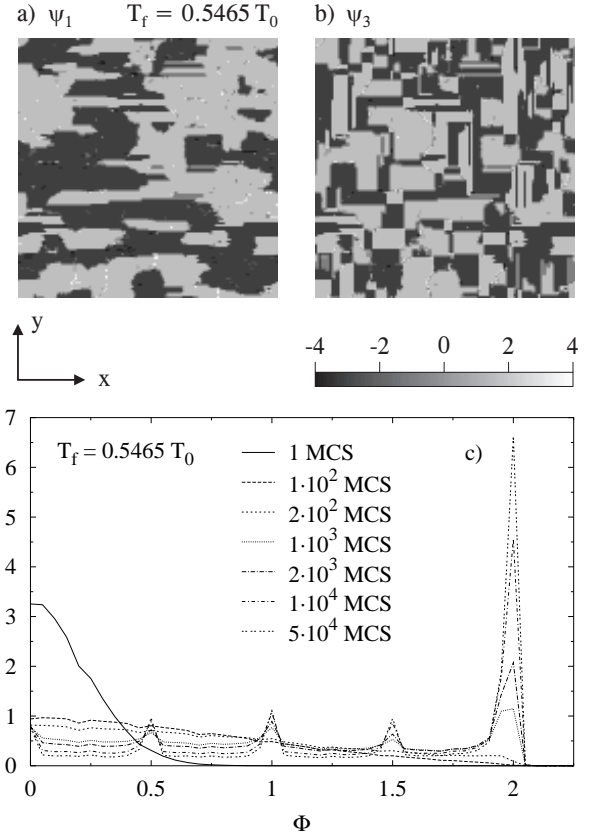


FIG. 3: Continuous ordering in a system of $128 \times 128 \times 128$ fcc-cells at $T_f = 0.5465 T_0 < T_{sp}$. (a) ψ_1 and (b) ψ_3 patterns at a time $t = 7 \times 10^3$ MCS after the quench from random initial conditions. Two types of domain walls are clearly shown. (c) Histograms of corresponding Φ values calculated at a series of times after the quench.

practically the whole system is already ordered and, as illustrated by curves for $t = 2 \cdot 10^4$ and $5 \cdot 10^4$ MCS, the distribution of Φ changes very little with time. At that stage coarsening processes take place.

In contrast to the above sequence of events, deep quenches ($T_f < T_{sp}$) result in continuous ordering, in which shortly after the quench the whole volume of the system decomposes into ordered domains. As a representative example Figs. 3a and 3b display distributions of ψ_1 and ψ_3 , respectively, for an xy -section through the system at $t = 7 \cdot 10^3$ MCS after a quench to $T_f = 0.5465 T_0$. The two types of domain walls, that may be formed in the system,^{2,12} show up in Figs. 3a and 3b. The low-energy interfaces appear there as straight lines parallel to the x or y -axis. Across each of these lines ψ_1 and ψ_3 , or ψ_2 and ψ_3 simultaneously change sign across line-intervals parallel, to the x or y -axes, respectively. Within the simple model used in this paper, formation of such walls costs no energy and therefore they are very stable. The curved interfaces seen in Fig. 3a consist of sectors of high-energy domain walls across which ψ_1 and ψ_2 change sign simultaneously. The histograms of Φ -values obtained after

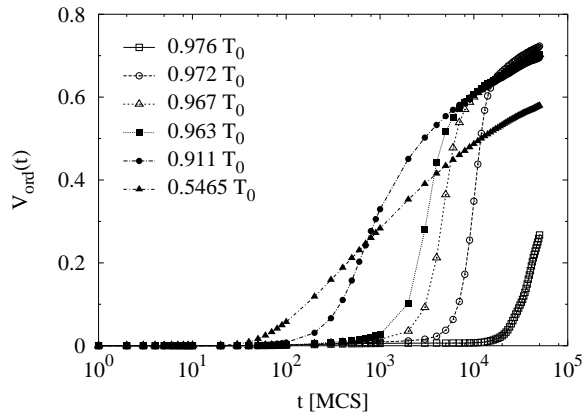


FIG. 4: Volume fraction, V_{ord} , of an ordered phase ($\Phi > 1.5$) as a function of time after the quench for a series of temperatures T_f .

averaging over 10 independent runs for $T_f = 0.5465 T_0$ are shown in Fig. 3c for a sequence of time intervals after the quench. There, in contrast to Fig. 2c, the initial peak at $\Phi = 0$ spreads out within the first 100 MCS and the maximum at $\Phi \simeq 2$ starts to grow by 200 MCS to reach a considerable height already at $2 \cdot 10^3$ MCS. The $\Phi \simeq 2$ peak is very narrow, indicating a nearly perfect local order in the system. Additional small, sharp peaks at multiples of $\Phi = 0.5$ may be traced back to the domain walls that cross some of the blocs of $4 \times 4 \times 4$ fcc-cells used to prepare Fig. 3c. Slow coarsening processes, which in this case set in already for $t > 2 \cdot 10^3$ MCS result in considerable sharpening of the main $\Phi \simeq 2$ peak.

To better illustrate the differences between the two ordering scenarios described above we show in Fig. 4 how V_{ord} , the volume fraction of the ordered phase, grows with time for a number of final temperatures. There, we counted as ordered all the blocs (of $4 \times 4 \times 4$ fcc-cells each) for which $\Phi > 1.5$. The character of $V_{ord}(t)$ changes from a slowly increasing function of t for $T_f \leq 0.911 T_0$ to a sharp, nearly stepwise growth after some incubation time for $T_f > 0.972 T_0$.

In the next two sections we analyze in more detail the incubation time and the long time coarsening processes.

IV. INCUBATION TIME

In the preceding section we introduced the incubation time τ_{inc} as the characteristic time interval between the quench and the observed growth of ordered domains in the case of metastability, $T_f > T_{sp}$. Let us now look more precisely at the processes that take place in the system within the initial stages of ordering. One relevant quantity here is the excess energy, $\Delta E(t) = E(t) - E(\infty)$, defined as the difference between the actual energy of the system, $E(t)$, and the energy it would reach after complete equilibration, $E(\infty)$. This means that we iden-

tify $E(\infty)$ with the energy of a single ordered domain of the size of the whole system, equilibrated at T_f . In Figure 5a $\Delta E(t)$ per lattice site is shown for a number of final temperatures T_f . Initially, the relaxation of $\Delta E(t)$ depends on temperature only weakly. Then, after about 20 MCS, the curves in Fig. 5a split due to a considerable slowing down of the relaxation rate with growing temperature. In turn, for shallow quenches, ordering proceeds in three stages, as displayed already in Fig. 2c. First, the system remains disordered up to a certain incubation time τ_{inc} . The metastability of the ordered phase is reflected by plateaus in $\Delta E(t)$, which develop near $T_f \simeq T_{sp}$, and extend with increasing T_f . Second, $\Delta E(t)$ drops markedly when overcritical nuclei are produced by thermal fluctuations. We define $\tau_{inc}(T)$ as precisely that moment after the quench at which, for a given temperature T , $\Delta E(t)$ drops notably (by about 10 percent) below its plateau-value. The ordered nuclei formed within the incubation time grow against the disordered bulk until, in a third stage, ordered regions meet and slow coarsening processes set in.

In addition to $\Delta E(t)$, we also show in Figure 5b and 5c how the corresponding first moments of the structure factors $S_\alpha(k_x, k_y, k_z, t)$ change with time. To account for the anisotropy illustrated in the domain patterns in Fig. 3a and b, we consider the two kinds of structure factors

$$S_{\parallel}(k, t) = \frac{1}{3}(S_1(k, 0, 0, t) + S_2(0, k, 0, t) + S_3(0, 0, k, t)), \quad (4)$$

and

$$S_{\perp}(k, t) = \frac{1}{N_k} \sum_{q_1^2 + q_2^2 = k^2} (S_1(0, q_1, q_2, t) + S_2(q_1, 0, q_2, t) + S_3(q_1, q_2, 0, t)), \quad (5)$$

where N_k denotes here the number of (q_1, q_2) pairs that fulfill $q_1^2 + q_2^2 = k^2$, as well as their first moments

$$k_{\parallel}(t) = \frac{\sum_{k>0} k S_{\parallel}(k, t)}{\sum_{k>0} S_{\parallel}(k, t)}, \quad (6)$$

$$k_{\perp}(t) = \frac{\sum_{k>0} k S_{\perp}(k, t)}{\sum_{k>0} S_{\perp}(k, t)}. \quad (7)$$

In Eq. (6) k denotes one wave-vector component, see Eq. (4), while in Eq. (7) k is defined as in Eq. (5). Clearly, $S_{\parallel}(k, t)$ is determined by structural modulations due to high-energy walls, which are reflected, for example, by sign-changes of ψ_1 when going along the x -axis, see Fig. 2. The quantity k_{\parallel} therefore characterizes the inverse distance between such walls in one symmetry direction. On the other hand, S_{\perp} is sensitive to the two-dimensional network of low-energy walls, and k_{\perp} gives the inverse distance between such walls, cf. Fig. 3.

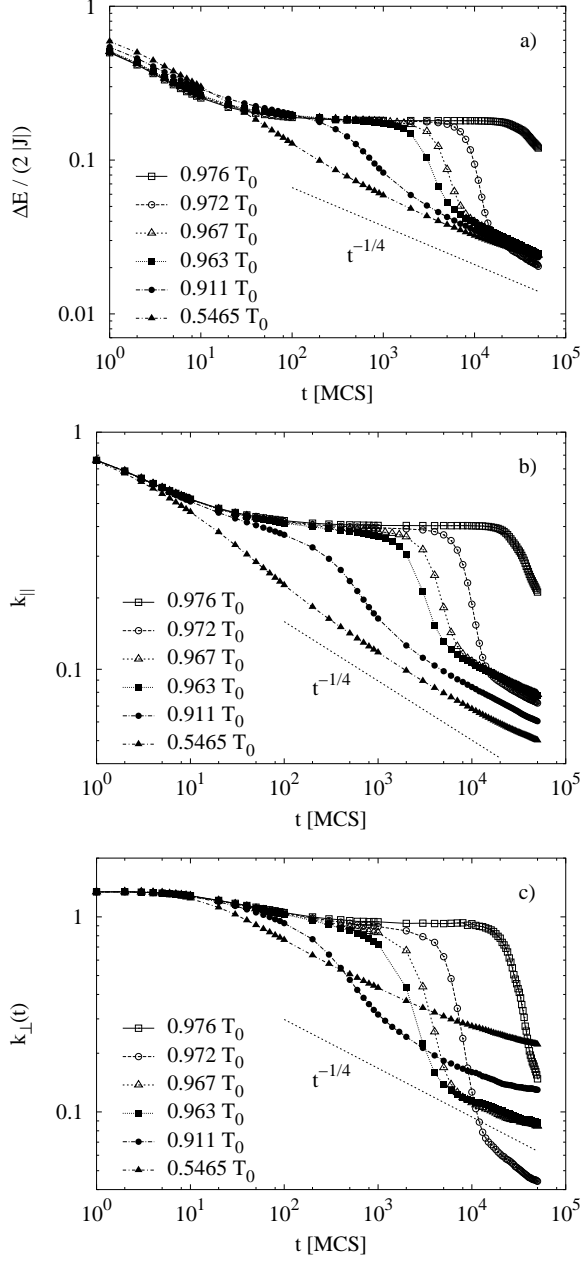


FIG. 5: Excess energy per lattice site ΔE (a), and the first moments $k_{||}(t)$ (b) and $k_{\perp}(t)$ (c) of the structure factors $S_{||}(k, t)$ and $S_{\perp}(k, t)$ as functions of time after the quench, calculated for a series of final temperatures T_f .

Curves displayed in all three parts of Figure 5 are strikingly similar in form, confirming that relaxation processes are indeed dominated by ordered domains growing in size. Moreover, ΔE , $k_{||}$ and k_{\perp} , all start to drop below their plateau-values at the same moment after the quench. This fact corroborates our linking the plateaus in $\Delta E(t)$ to the temperature-dependent incubation time for the formation of overcritical ordered nuclei. In accord with the spatial patterns shown in Figs. 2a, 3a and

3b, where high-energy walls are much further apart from each other than the low-energy ones, $k_{||}(t)$ is in most cases considerably smaller than $k_{\perp}(t)$ calculated at the same temperature.

There are two effects restricting the range of $\tau_{inc}(T_f)$ accessible to simulations. First, the system size L must be considerably larger than the size of overcritical nuclei which are formed at temperature T_f . Second, obtaining smooth curves in Fig. 5 requires a sufficiently large number of nucleation events within the maximum computation time t_{max} . Again, this becomes increasingly difficult to fulfill with growing T_f because both τ_{inc} and the dispersion of nucleation times over the different samples strongly increase with T_f . Comparing our results up to $t_{max} = 5 \cdot 10^4$ for lattices of size $L=96$ and $L=128$ we find $T_f \simeq 0.973 T_0$ to be roughly the highest temperature for which τ_{inc} can be determined in a reliable way.

Results of our simulations for $\tau_{inc}(T)$, plotted in Fig. 6, are consistent with the expression

$$\ln \tau_{inc} \propto (T_0 - T_f)^{-2}, \quad (8)$$

which is similar in form to the nucleation rates obtained within classical nucleation theory^{5,18} and Monte Carlo simulations.^{5,6} Note that the data point with $T_f/T_0 = 0.911$ falls well below the spinodal, but in Fig. 2 there still exists a shoulder at that temperature as a remnant of the plateaus at higher temperatures.

Incubation times for Cu_3Au have been measured by Noda et al.¹⁹ from the width $\Gamma \propto k_{\perp}(t)$ of the (110) X-ray diffraction peak. Close to T_0 the width as a function of time develops plateaus qualitatively similar to Fig. 5c. Their data, however, refer to $T_f/T_0 > 0.981$, whereas ours are for $T_f/T_0 \lesssim 0.976$. Also one should note that experimentally the ratio T_{sp}/T_0 may be sample-dependent. Because of the sensitivity of τ_{inc} to temperature differ-

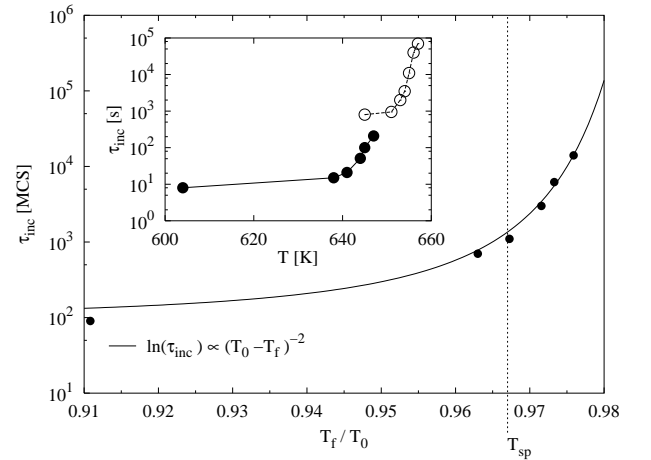


FIG. 6: Incubation times τ_{inc} versus reduced temperature T_f . The inset shows the same data (full symbols) after conversion to the physical time scale as described in the text, together with incubation times measured¹⁹ in Cu_3Au (open symbols).

ences with respect to T_{sp} , this introduces considerable uncertainties in our comparison. Nevertheless it is interesting to present experiments and simulations in one plot, as done in the inset of Fig. 6. There the simulation data were linked to the physical time scale exactly in the manner described towards the end of section II. Both sets of data display a remarkable similarity with respect to the order of magnitude in time and their trend with temperature (and even seem to be a continuation of each other). We conclude that the connection between time scales for diffusion (see section II) and nucleation as implied by our algorithm roughly agrees with experiment.

V. COARSENING REGIME AND SCALING

As pointed out in the preceding sections, the distances between high- and low-energy walls define two different length scales. Moreover, the high-energy walls that are much further apart from each other than the low-energy ones, are also less stable. As a consequence, we expect direction-dependent scaling laws to hold for the structure factors $S_\alpha(\vec{k}, t)$. This is made explicit by considering the functions S_\parallel and S_\perp introduced in Eqs. 4 and 5. Due to their definitions we expect these structure factors to obey scaling laws for one-dimensional and two-dimensional systems, respectively. This is verified by our simulations at $T_f = 0.5465 T_0$, i. e. in the case of continuous ordering. As shown by the 1d and 2d scaling plots in Figs. 6a and 6b, the data taken for a number of times $t \geq 500$ MCS after the quench indeed collapse onto single master curves. Moreover, the decay of both quantities at large k appears to be consistent with Porod's law in $d = 1$ and $d = 2$, respectively,^{20,21}

$$k_\parallel(t) S_\parallel(k, t) \propto (k/k_\parallel(t))^{-2}, \quad (9)$$

$$k_\perp^2(t) S_\perp(k, t) \propto (k/k_\perp(t))^{-3}. \quad (10)$$

We now ask whether the same scaling laws apply to the results for $T_f > T_{sp}$, i. e. to the case of thermally activated ordering. Figure 8 contains the corresponding plots of $S_\parallel(k, t)$, part (a), and $S_\perp(k, t)$, part (b), calculated for $T_f = 0.972 T_0$ at times $t > \tau_{inc}$. In both parts of the figure scaling regimes are observed which are consistent with Eqs. (9) and (10) in an intermediate range of k -values. Both S_\parallel and S_\perp , however, develop tails at large k which show significant deviations from scaling. These deviations can be traced back to irregular shapes of overcritical nuclei growing against the disordered bulk (cf. Fig. 2). Such highly structured grain boundaries eventually meet, leading to likewise structured domain walls when the regime of slow coarsening is reached. Small inclusions of disordered phase still remain trapped between boundaries of ordered grains for quite

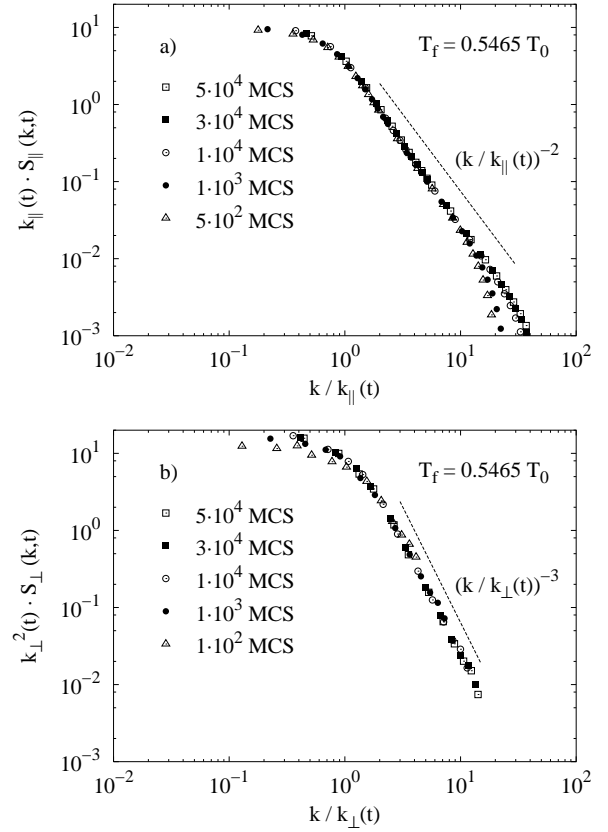


FIG. 7: Scaled structure factors $k_\parallel S_\parallel(k, t)$ (a) and $k_\perp^2 S_\perp(k, t)$ (b) calculated for $T_f = 0.5465 T_0 < T_{sp}$; the slopes of the dashed straight lines represent a decay according to $(k/k_\parallel)^{-2}$ (a), and $(k/k_\perp)^{-3}$ (b).

a long time after the onset of coarsening processes in the bulk of the crystal.

Closer inspection of our data near the onset of those tails reveals that indeed, with increasing time t , the validity of Porod's law extends to larger k in both parts of Figure 8. We may take this as indication that Porod's law, defined by Eqs. (9) and (10), will dominate in the late stages of continuous as well as thermally activated ordering processes.

The last point we like to address concerns the observed growth rates of the characteristic domain-size, $l(t)$. Since the transition considered here is described by a set of non-conserved order parameters ψ_1 through ψ_3 , one might expect that ordered domains grow according to the Lifshitz–Allen–Cahn law $l(t) \propto t^\nu$ with $\nu = 1/2$.^{7,8} Experiments on Cu₃Au indeed were interpreted in terms of this conventional growth law.^{19,22,23} In this context, however, one should be aware of the fact that systems of the type considered may show effective growth exponents during relaxation different from the Lifshitz–Allen–Cahn law. In the case of a vacancy mechanism effective exponents $\nu > 1/2$ in principle can arise in models based on a non-conserved order parameter. In these studies,^{24,25} an increased ν was ascribed to an accumulation of va-

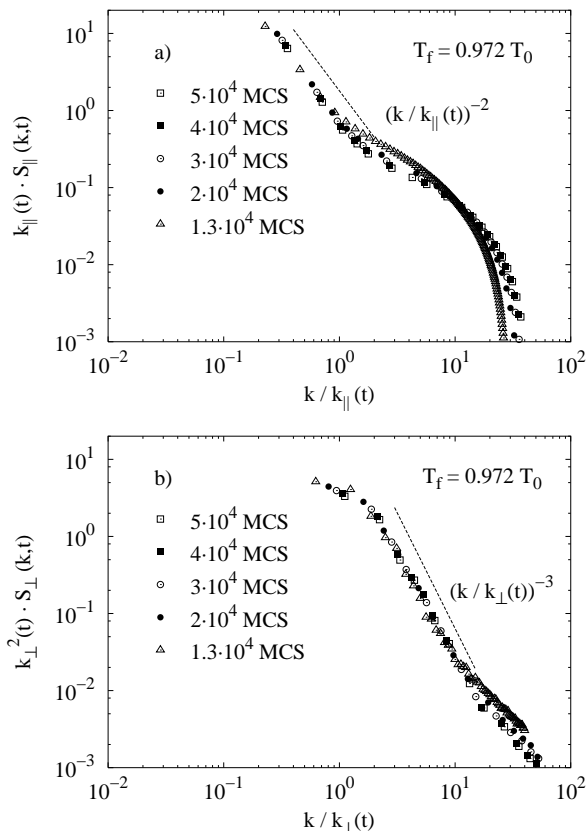


FIG. 8: Same as in Fig. 7 but for $T_f = 0.972 T_0 > T_{sp}$.

cancies within the domain boundaries, leading to an enhancement of the interfacial dynamics. For the present model we have verified, however, that the interaction parameters chosen do not favor segregation of vacancies in the domain boundaries.²⁶ Another modification of the Lifshitz–Allen–Cahn law that can act in the opposite direction results from local changes in composition within antiphase boundaries so that the ordering process gets coupled to a (slow) conserved order parameter component.

In our simulations we systematically observe effective growth exponents $\nu \simeq 1/4$ or even smaller (cf. Fig. 5 and Kessler *et al.*⁴). Moreover, within our accessible computing times ($3 \cdot 10^4 - 5 \cdot 10^4$ MCS), these exponents depend slightly on temperature. One possible source of these differences between simulations and the experimental data ($\nu \simeq 1/2$) seems to be the existence of the low-energy type-I walls. Specifically, let us recall that our model contains only nearest neighbor interactions, so that type-I walls have zero energy and thus are extremely stable. It has been suggested previously that such a situation may lead to $\nu = 1/4$.^{27,28} Moreover, the present model does imply a coupling of the non-conserved order parameters to the conserved density ψ_0 . This coupling becomes active within type-II walls. The relaxation of a modified composition within type-II walls is slowed down fur-

ther because type-II walls are interconnected via type-I walls which have fixed ψ_0 and do not allow any exchange of composition. The slight upward bending of the low-temperature data in Fig. 5 at the longest times, indicating an even slower growth, might be interpreted in this way, although this point needs to be clarified in further studies.

VI. SUMMARY AND CONCLUSIONS

Implementing the vacancy mechanism in a model for the atomic dynamics in A_3B -type fcc-alloys, we investigated the growth of ordered domains after a temperature quench below the transition temperature T_0 . Depending on the depth of the quench we observe two clearly distinct ordering-scenarios: thermally activated nucleation of the ordered phase for shallow quenches, $T_0 > T_f > T_{sp}$, and spinodal ordering, when $T_f < T_{sp}$. Here, the spinodal temperature T_{sp} was taken over from independent simulations at equilibrium.

In the case of thermally activated processes there is some characteristic incubation time, τ_{inc} , after which a small fraction of the system is covered by overcritical nuclei. Detailed simulation results for τ_{inc} , based on vacancy–atom exchange, were presented. The time period $t < \tau_{inc}$ manifests itself in plateau regions for energy relaxation and for the size of ordered domains, when plotted versus t . Clearly, τ_{inc} is expected to diverge as T_f approaches T_0 from below. Within the simple model investigated here and the available maximum computing time, τ_{inc} grows more than 260 times in a narrow temperature interval above T_{sp} – from about 90 MCS at $T_f = 0.911 T_0$ to roughly $24 \cdot 10^3$ MCS at $T_f = 0.976 T_0$. In comparison with measurements¹⁹ of τ_{inc} this seems to constitute the correct order of magnitude when Monte Carlo times are converted to physical times with the help of experimental tracer diffusion coefficients. In the coarsening regime we observed growth of the characteristic domain-size that was clearly slower than the conventional $t^{1/2}$ -law expected for curvature driven processes in the presence of non-conserved order parameters. This may be due to the enhanced stability of the low-energy domain walls in the case of nearest-neighbor effective interactions assumed in our model. The enhanced stability of low energy walls leads to strong anisotropies of the domain-shapes observed in our system, and furthermore, to independent scaling laws for the correlation functions $S_{\parallel}(k, t)$ and $S_{\perp}(k, t)$. These two functions scale according to Porod’s laws for dimensions one and two, respectively, when $T_f \ll T_{sp}$. For $T_f > T_{sp}$ strong deviations from these scaling laws are observed in the region of large k -values, due to highly structured domain walls which originate from the stage of fast growth of ordered nuclei against disordered bulk.

Acknowledgments

Helpful discussions with P. Maass are gratefully acknowledged. This work was supported in part by the

Deutsche Forschungsgemeinschaft, SFB 513.

-
- ¹ S. M. Allen and J. W. Cahn, *Acta Metal.* **24**, 425 (1976).
 - ² Z.-W. Lai, *Phys. Rev.* **B41**, 9239 (1990).
 - ³ C. Frontera, E. Vives, T. Castán, and A. Planes, *Phys. Rev.* **B55**, 212 (1997).
 - ⁴ M. Kessler, W. Dieterich, and A. Majhofer, *Phys. Rev.* **B64**, 125412-1 (2001).
 - ⁵ K. Binder and D. Stauffer, *Adv. Phys.* **25**, 343 (1976) and references quoted therein.
 - ⁶ M. Acharyya and D. Stauffer, *Eur. Phys. J.* **B5**, 571 (1998).
 - ⁷ I. M. Lifshitz, *Sov. Phys. JETP* **15**, 939 (1962); *J. Exp. Theor. Phys. (U.S.S.R.)* **42**, 1354 (1962).
 - ⁸ S. M. Allen and J. W. Cahn, *Acta Metall.* **27**, 1085 (1979).
 - ⁹ K. Binder, *Phys. Rev. Lett.* **45**, 811 (1980).
 - ¹⁰ W. Schweika and D. P. Landau, *Monte Carlo Studies of Surface-Induced Ordering in Cu₃Au Type Alloy Models*, Springer Proceedings in Physics, Vol. 83, Eds D. P. Landau, K. K. Mon, and H.-B. Schüttler, Springer-Verlag, Berlin, Heidelberg, 1998, pp 186–190.
 - ¹¹ B. E. Warren, *X-Ray Diffraction*, Addison-Wesley Publishing Company, Reading Massachusetts, 1969, pp 206–247.
 - ¹² R. Kikuchi and J. W. Cahn, *Acta Metall.* **27**, 1337 (1979).
 - ¹³ As a result, the ground state of that model in fact is infinitely degenerate.
 - ¹⁴ M. Yamaguchi and Y. Shirai in *Physical Metallurgy and Processing of Intermetallic Compounds*, Eds N. S. Stoloff and V. K. Sikka, Chapman and Hall, New York, 1996. The data on vacancy formation in the disordered phase of Cu₃Au reported in this paper lead to $c^V \simeq 10^{-7}$ for the average vacancy concentration at T_0 .
 - ¹⁵ T. Heumann, and T. Rottwinkel, *J. Nucl. Mater.* **69–70**, 567 (1978).
 - ¹⁶ S. Benci, G. Gasparrini, E. Germagnoli, and G. Schianchi, *J. Phys. Chem. Solids* **26**, 687 (1965).
 - ¹⁷ K. Binder, *Rep. Progr. Phys.* **50**, 783 (1987) and references quoted therein.
 - ¹⁸ A. M. Zettlemoyer, *Nucleation*, Dekker, New York, 1969.
 - ¹⁹ Y. Noda, S. Nishihara, and Y. Yamada, *J. Phys. Soc. Japan* **53**, 4241 (1984).
 - ²⁰ G. Porod, in *Small Angle X-Ray Scattering*, Eds O. Glatter and L. Kratky, Academic Press, New York, 1982.
 - ²¹ In their simulations of the ordering kinetics in Cu₃Au for $T_f < T_{sp}$ Frontera *et al.*³ noticed direction-dependent scaling and deviations of the structure factors from the 3-dimensional form of Porod's law.
 - ²² R. F. Shannon, Jr., S. E. Nagler, C. R. Harkless, and R. M. Nicklow *Phys. Rev.* **B46**, 40 (1992).
 - ²³ H. Konishi and Y. Noda, in *Dynamics of Ordering Processes in Condensed Matter*, Eds S. Komura and H. Furukawa, Plenum Press, New York, 1989, p.309.
 - ²⁴ E. Vives, and A. Planes, *Phys. Rev. Lett.* **68**, 812 (1992).
 - ²⁵ P. Fratzl, and O. Penrose, *Phys. Rev.* **B55**, R6101 (1997).
 - ²⁶ M. Porta, E. Vives, and T. Castan, *Phys. Rev.* **B60**, 3920 (1999).
 - ²⁷ T. Castan, and P.-A. Lindgård, *Phys. Rev.* **B43**, 956 (1991).
 - ²⁸ P. A. Deymier, J. O. Vasseur, and L. Dobrzyński, *Phys. Rev.* **B55**, 205 (1997).